Applied Numerical Mathematics 132 (2018) 35–50

Contents lists available at ScienceDirect

Applied Numerical Mathematics

www.elsevier.com/locate/apnum

Construction and comparison of multidimensional spectral variational integrators and spectral collocation methods

Yiqun Li [a,b,*], Boying Wu [b], Melvin Leok [c]

[a] State Key Laboratory of Digital Manufacturing Equipment and Technology, Huazhong University of Science and Technology, Wuhan, 430074, PR China
[b] Department of Mathematics, Harbin Institute of Technology, Harbin 150001, PR China
[c] Department of Mathematics, University of California at San Diego, La Jolla, CA 92093, USA

ARTICLE INFO

Article history:
Received 20 September 2017
Accepted 16 May 2018
Available online 26 May 2018

Keywords:
Lagrangian mechanics
Spectral collocation methods
Spectral variational integrators
Linear stability

ABSTRACT

In this paper, we construct numerical schemes for spectral collocation methods and spectral variational integrators which converge geometrically. We present a systematic comparison of how spectral collocation methods and Galerkin spectral variational integrators perform in terms of their ability to reproduce accurate trajectories in configuration and phase space, their ability to conserve momentum and energy, as well as the linear stability of these methods when applied to some classical Hamiltonian systems.

1. Introduction

Hamiltonian systems are omnipresent in scientific and technical applications and play an important role in many different fields, such as celestial mechanics [3], quantum mechanics [11], molecular dynamics [7], control theory [15], etc. Ideally, numerical schemes for the simulation of Hamiltonian systems should not only reproduce the solutions accurately and efficiently, but also preserve as many geometric invariants of the original system as possible. Variational integrators (VI) [12,4] are well-known as they are symplectic, momentum preserving and nearly energy preserving for exponentially long times. Spectral collocation methods (SC) [16,17,10] are a popular choice for the construction of numerical approximations for problems with smooth solutions, as they can achieve geometric rates of convergence and have a relatively small memory footprint. Spectral variational integrators (SVI) [5] inherit almost all the benefits of both methods. Comparisons of Euler methods and Runge–Kutta methods with their corresponding symplectic counterparts are discussed in [4,1,12]. It would be interesting to compare the performance of spectral variational integrators with spectral collocation schemes to see if any additional benefits arise from constructing spectral schemes using a variational approach. The procedures for constructing SVI and SC are illustrated in Fig. 1. The paradigms underlying spectral variational integrators and spectral collocation methods for the numerical solution of dynamical systems are straightforward. Approximate solutions of Lagrangian systems are represented by finite vectors of their values at certain points such as Chebyshev–Gauss–Lobatto points. Each such vector defines a global interpolant and operations on the analytic solutions of the proposed Lagrangian systems are replaced by the corresponding operations on the interpolants. The main difference between the two constructions is that SC performs the

* Corresponding author at: State Key Laboratory of Digital Manufacturing Equipment and Technology, Huazhong University of Science and Technology, Wuhan, 430074, PR China.
E-mail addresses: liyiqun@hust.edu.cn (Y. Li), mathwby@hit.edu.cn (B. Wu), mleok@math.ucsd.edu (M. Leok).

https://doi.org/10.1016/j.apnum.2018.05.010
0168-9274/

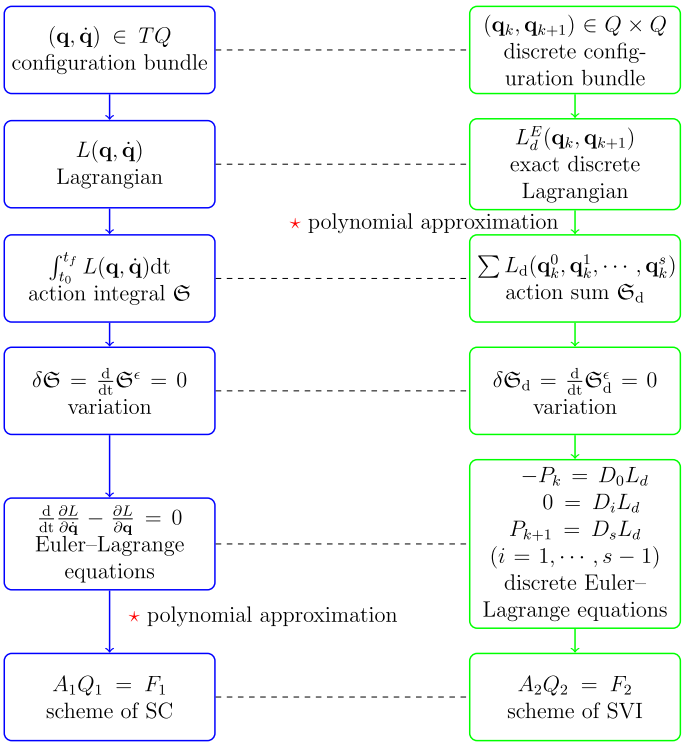

Fig. 1. Construction procedures for SC (left column) and SVI (right column).

variation in Hamilton's principle first and then discretizes the resulting Euler–Lagrange equations, whereas SVI discretizes Hamilton's principle first and then performs the variation of the resulting discrete Hamilton's principle.

1.1. Discrete Lagrangian mechanics and variational integrators

Considering mechanical systems that evolve on an n-dimensional configuration manifold Q with generalized coordinates $q^i, i = 1, ..., n$, the Lagrangian $L : TQ \times \Delta \to \mathbb{R}$ of the proposed mechanical systems are defined as the difference between the kinetic energy and the potential energy, i.e.,

$$L(\mathbf{q}, \dot{\mathbf{q}}, t) = T(\mathbf{q}, \dot{\mathbf{q}}, t) - V(\mathbf{q}, \dot{\mathbf{q}}, t),$$

where Δ represents an interval in the time axis, and where T and V denote the total kinetic and potential energy of the system, respectively. Define the action $\mathfrak{S} : C^2([t_0, T], Q) \to \mathbb{R}$ of the Lagrangian system as the following functional

$$\mathfrak{S} = \int_{t_0}^{T} L(\mathbf{q}(t), \dot{\mathbf{q}}(t), t)\mathrm{d}t,$$

where $(\mathbf{q}, \dot{\mathbf{q}}) \in TQ$ is a smooth curve between states $(\mathbf{q}(t_0), \dot{\mathbf{q}}(t_0))$ and $(\mathbf{q}(T), \dot{\mathbf{q}}(T))$. According to Hamilton's principle, we know that the true trajectory $\mathbf{q} \in C^2([t_0, T], Q)$ is the stationary point of the functional $\mathfrak{S}$ with fixed endpoints $\mathbf{q}(t_0)$ and $\mathbf{q}(T)$, i.e.,

$$\delta\mathfrak{S} = \delta \int_{t_0}^{T} L(\mathbf{q}(t), \dot{\mathbf{q}}(t), t)\mathrm{d}t = 0, \tag{1}$$

which yields the Euler–Lagrange (EL) equations,

$$\frac{\mathrm{d}}{\mathrm{d}t}\frac{\partial L}{\partial \dot{\mathbf{q}}} - \frac{\partial L}{\partial \mathbf{q}} = 0. \tag{2}$$

The formulation of Lagrangian mechanics in discrete time is mainly based on a discrete analogue of Hamilton's principle. Divide the total time interval $[t_0, T]$ into N subintervals of equal length h. The discrete Lagrangian $L_d : Q \times Q \times \mathbb{R} \to \mathbb{R}$ is an approximation of the exact discrete Lagrangian over each time interval $[kh, (k+1)h]$, i.e.,

$$L_d(\mathbf{q}_k, \mathbf{q}_{k+1}; h) \approx L_d^E(\mathbf{q}_k, \mathbf{q}_{k+1}; h) = \underset{\substack{\mathbf{q}\in C^2([kh,(k+1)h],\,Q)\\ \mathbf{q}(kh)=\mathbf{q}_k,\mathbf{q}((k+1)h)=\mathbf{q}_{k+1}}}{\operatorname{ext}} \int_{kh}^{(k+1)h} L(\mathbf{q}(t), \dot{\mathbf{q}}(t))\mathrm{d}t. \tag{3}$$

The exact discrete Lagrangian L_d^E is associated with Jacobi's solution of the Hamilton–Jacobi equation, and cannot typically be computed. In the next section, we will show how it can be approximated by choosing a finite-dimensional function space and a quadrature formula. Then, the discrete action sum $\mathfrak{S}_d : Q^{N+1} \to \mathbb{R}$ can be constructed as

$$\mathfrak{S}_d(\mathbf{q}_0, \mathbf{q}_1, ..., \mathbf{q}_N) = \sum_{k=0}^{N-1} L_d(\mathbf{q}_k, \mathbf{q}_{k+1}).$$

The discrete Hamilton's principle states that

$$\delta\mathfrak{S}_d = 0,$$

for variations of the discrete curve $\mathbf{q}_0, \mathbf{q}_1, ..., \mathbf{q}_N$ that keep the endpoints fixed. This yields the discrete Euler–Lagrange equations,

$$D_2L_d(\mathbf{q}_{k-1}, \mathbf{q}_k) + D_1L_d(\mathbf{q}_k, \mathbf{q}_{k+1}) = 0, \qquad k = 1, 2, \ldots, N-1, \tag{4}$$

and implicitly defines the discrete Lagrangian map $F_{L_d}^{(h)} : (\mathbf{q}_{k-1}, \mathbf{q}_k) \mapsto (\mathbf{q}_k, \mathbf{q}_{k+1})$. Here, D_1 and D_2 denote partial derivatives of L_d with respect to the first and second variables, respectively. Equation (4) is equivalent to the implicit discrete Euler–Lagrange (IDEL) equations,

$$\mathbf{p}_k = -D_1L_d(\mathbf{q}_k, \mathbf{q}_{k+1}), \qquad \mathbf{p}_{k+1} = D_2L_d(\mathbf{q}_k, \mathbf{q}_{k+1}), \qquad k = 0, 1, \ldots, N-1, \tag{5}$$

which implicitly defines the discrete Hamiltonian map $\tilde{F}_{L_d}^{(h)} : (\mathbf{q}_k, \mathbf{p}_k) \mapsto (\mathbf{q}_{k+1}, \mathbf{p}_{k+1})$. From equation (5), we can see that the discrete Lagrangian L_d is a Type I generating function of the symplectic map $\tilde{F}_{L_d}^{(h)}$. The discrete Lagrangian and Hamiltonian maps describe numerical integration schemes that are referred to as variational integrators, which are automatically symplectic and exhibit excellent long-time energy behavior. If the discrete Lagrangian L_d is G-invariant under the diagonal action, i.e., $L_d(g\mathbf{q}_k, g\mathbf{q}_{k+1}) = L_d(\mathbf{q}_k, \mathbf{q}_{k+1})$, for every $g \in G$, then, by the discrete Noether's theorem, the variational integrator also preserves the discrete momentum map associated with the G action. The accuracy of the proposed structure-preserving numerical scheme is closely related to the approximation accuracy of discrete Lagrangian L_d with respect to the exact discrete Lagrangian L_d^E. Specifically, this relationship is characterized by the following theorem.

Theorem 1.1. (Variational error analysis [12]) *Given a regular Lagrangian L and corresponding Hamiltonian H, the following are equivalent for a discrete Lagrangian L_d:*

(1) *the discrete Hamiltonian map for L_d is of order r,*
(2) *the discrete Legendre transforms of L_d are of order r,*
(3) *L_d approximates the exact discrete Lagrangian L_d^E with order r.*

2. Spectral variational integrators

Without loss of generality, we consider mechanical systems defined on the total time interval $[0, T]$ with Lagrangian $L : TQ \times \Delta \to \mathbb{R}$. We divide the time interval $[0, T]$ into N subintervals of equal length h,

$$[0, T] = \bigcup_{k=0}^{N-1} [kh, (k+1)h], \quad N = T/h,$$

and apply spectral variational integrators to solve the Lagrangian system in each subinterval.

Since the accuracy of a variational integrator is determined by how well the discrete Lagrangian L_d approximates the exact discrete Lagrangian L_d^E, the motivating idea of spectral variational integrators is to approximate the numerically non-computable exact discrete Lagrangian L_d^E with a highly-accurate computable discrete Lagrangian L_d by applying Lagrange–Chebyshev interpolation. Specifically, for a given Lagrangian $L : TQ \times \Delta \to \mathbb{R}$, the spectral discrete Lagrangian (SDL) is constructed using the following procedure:

1. Choose an $(s+1)$-dimensional polynomial space $\mathbb{P}^s([kh, (k+1)h], Q) \subset C^2([kh, (k+1)h], Q)$ generated by Lagrange basis polynomials $\{l_{\nu,s}(t)\}_{\nu=0}^{s}$ based at the points $c_\nu = \frac{(2k+1)h}{2} - \frac{h}{2}\cos\left(\frac{\nu\pi}{s}\right)$, where c_ν are the Chebyshev–Gauss–Lobatto (CGL) points $x_\nu = -\cos(\frac{\nu\pi}{s})$, $0 \le \nu \le s$, rescaled and shifted from $[-1, 1]$ to $[kh, (k+1)h]$. Then, as illustrated in Fig. 2,

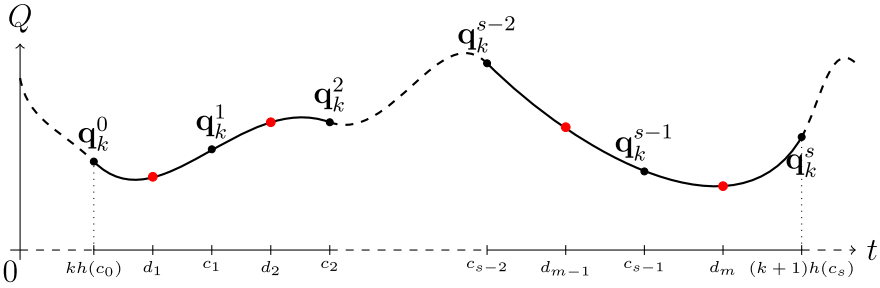

Fig. 2. The red dots represent the quadrature points, which may or may not be the same as the interpolation points which are represented by black dots. (For interpretation of the colors in the figure(s), the reader is referred to the web version of this article.)

the approximation of the solution curve $(\mathbf{q}, \dot{\mathbf{q}}) \in TQ$ in the interval $[kh, (k+1)h]$ can be expressed in the following form

$$\mathbf{q}(t) \approx \sum_{\nu=0}^{s} \mathbf{q}_k^\nu l_{\nu,s}(t); \quad \dot{\mathbf{q}}(t) \approx \sum_{\nu=0}^{s} \mathbf{q}_k^\nu \dot{l}_{\nu,s}(t),$$

where $\mathbf{q}(t) = [q_1(t), q_2(t), \cdots, q_n(t)]$, $\dot{\mathbf{q}}(t) = [\dot{q}_1(t), \dot{q}_2(t), \cdots, \dot{q}_n(t)]$;

2. Choose a quadrature rule (w_i, τ_i) to approximate the integral in the definition of the exact discrete Lagrangian, and extremize the quadrature approximation over curves in $\mathbb{P}^s([kh, (k+1)h], Q)$ satisfying the boundary conditions in order to obtain a computable discrete Lagrangian in each time interval $[kh, (k+1)h]$, $k = 0, \ldots, N-1$, i.e.,

$$\begin{aligned} L_d(\mathbf{q}_k = \mathbf{q}_k^0, \mathbf{q}_k^1, \cdots, \mathbf{q}_k^s = \mathbf{q}_{k+1}; h) &= \operatorname*{ext}_{\substack{\mathbf{q} \in \mathcal{C}^s([kh,(k+1)h], Q) \\ \mathbf{q}_k^0 = \mathbf{q}_k, \mathbf{q}_k^s = \mathbf{q}_{k+1}}} \frac{h}{2} \sum_{\mu=1}^{m} w_\mu L(\mathbf{q}(d_\mu), \dot{\mathbf{q}}(d_\mu)) \\ &= \operatorname*{ext}_{\substack{(\mathbf{q}_k^0, \mathbf{q}_k^1, \ldots, \mathbf{q}_k^s) \\ \mathbf{q}_k^0 = \mathbf{q}_k, \mathbf{q}_k^s = \mathbf{q}_{k+1}}} \frac{h}{2} \sum_{\mu=1}^{m} w_\mu L(\sum_{\nu=0}^{s} \mathbf{q}_k^\nu l_{\nu,s}(\tau_\mu), \frac{2}{h} \sum_{\nu=0}^{s} \mathbf{q}_k^\nu \dot{l}_{\nu,s}(\tau_\mu)), \end{aligned} \tag{6}$$

where d_μ are quadrature points in the interval $[kh, (k+1)h]$, $\tau_\mu = \frac{2}{h}(d_\mu - kh) - 1 \in [-1, 1]$ and the Lagrange basis polynomials $l_{\nu,s} : [-1, 1] \to \mathbb{R}$ are given by

$$l_{\nu,s}(\tau) = \prod_{0 \le \mu \le s, \mu \ne \nu} \frac{\tau - x_\mu}{x_\nu - x_\mu}. \tag{7}$$

In equation (6), we know that $\mathbf{q}_k^\nu$, $\nu = 1, \ldots, s-1$, are stationary points of the discretized action, which provide $s-1$ internal stage conditions:

$$D_\nu L_d(\mathbf{q}_k = \mathbf{q}_k^0, \mathbf{q}_k^1, \cdots, \mathbf{q}_k^s = \mathbf{q}_{k+1}; h) = 0, \quad \nu = 1, \ldots, s-1.$$

Here, $D_\nu L$ means the partial derivative of L with respect to $\mathbf{q}_k^\nu$. Combining these internal stage conditions with the implicit discrete Euler–Lagrange (IDEL) equations,

$$\mathbf{p}_k = -D_1 L_d(\mathbf{q}_k, \mathbf{q}_{k+1}), \qquad \mathbf{p}_{k+1} = D_2 L_d(\mathbf{q}_k, \mathbf{q}_{k+1}),$$

yield a system of nonlinear equations,

$$-\mathbf{p}_k = \sum_{\mu=1}^{m} w_\mu \Big[\frac{h}{2} l_{0,s}(\tau_\mu) \frac{\partial L}{\partial \mathbf{q}}(d_\mu) + \dot{l}_{0,s}(\tau_\mu) \frac{\partial L}{\partial \dot{\mathbf{q}}}(d_\mu) \Big], \tag{8a}$$

$$\mathbf{0} = \sum_{\mu=1}^{m} w_\mu \Big[\frac{h}{2} l_{\nu,s}(\tau_\mu) \frac{\partial L}{\partial \mathbf{q}}(d_\mu) + \dot{l}_{\nu,s}(\tau_\mu) \frac{\partial L}{\partial \dot{\mathbf{q}}}(d_\mu) \Big], \qquad \nu = 1, \ldots, s-1, \tag{8b}$$

$$\mathbf{p}_{k+1} = \sum_{\mu=1}^{m} w_\mu \Big[\frac{h}{2} l_{s,s}(\tau_\mu) \frac{\partial L}{\partial \mathbf{q}}(d_\mu) + \dot{l}_{s,s}(\tau_\mu) \frac{\partial L}{\partial \dot{\mathbf{q}}}(d_\mu) \Big], \tag{8c}$$

which define the discrete Hamiltonian map $(\mathbf{q}_k, \mathbf{p}_k) \mapsto (\mathbf{q}_{k+1}, \mathbf{p}_{k+1})$. Equations (8a) and (8b) can be written in the following matrix form:

$$A_k \mathcal{Q}_k + F_k = G_k, \tag{9}$$

where A_k is a $s \times (s+1)$ matrix and the entries are given by,

$$A_k^{i,j} = \frac{2}{h} \sum_{\mu=1}^{m} w_\mu \dot{l}_{i-1,s}(\tau_\mu) \dot{l}_{j-1,s}(\tau_\mu), \qquad i = 1, \ldots, s; \quad j = 1, \ldots, s+1,$$

$\mathcal{Q}_k$ is a $(s+1) \times n$ matrix

$$\mathcal{Q}_k = [\mathbf{q}_k^0, \mathbf{q}_k^1, \cdots, \mathbf{q}_k^s]^T,$$

F_k is a $s \times n$ matrix

$$\begin{aligned} F_k &= [\mathbf{f}_k^0, \mathbf{f}_k^1, \cdots, \mathbf{f}_k^{s-1}]^T \\ &= \Big[\frac{h}{2} \sum_{\mu=1}^{m} w_\mu l_{0,s}(\tau_\mu) \cdot \frac{\partial L}{\partial \mathbf{q}}, \frac{h}{2} \sum_{\mu=1}^{m} w_\mu l_{1,s}(\tau_\mu) \cdot \frac{\partial L}{\partial \mathbf{q}}, \cdots, \frac{h}{2} \sum_{\mu=1}^{m} w_\mu l_{s-1,s}(\tau_\mu) \cdot \frac{\partial L}{\partial \mathbf{q}}\Big]^T, \end{aligned}$$

and G_k is a $s \times n$ matrix

$$G_k = [-\mathbf{p}_k, \mathbf{0}_{(s-1)\times n}]^T.$$

As the initial value $\mathbf{q}_k^0$ can usually be obtained from the previous step, the dimension of (9) can be reduced by considering partitions $A_k = [A_k^0, A_k^\star]$ and $\mathcal{Q}_k = [\mathbf{q}_k^0, \mathcal{Q}_k^\star]^T$, where A_k^0 is the first column of matrix A_k, $A_k^\star$ is the remaining part of A_k, $\mathbf{q}_k^0$ is the first row of matrix $\mathcal{Q}_k$, $\mathcal{Q}_k^\star$ is the remaining part of $\mathcal{Q}_k$. Then, we have

$$A_k^\star \otimes I_n \mathrm{vec}(\mathcal{Q}_k^\star) + A_k^0 \otimes (\mathbf{q}_k^0)^T + \mathrm{vec}(F_k - G_k) = 0, \tag{10}$$

where I_n is the $n \times n$ identity matrix and

$$\begin{aligned} \mathrm{vec}(\mathcal{Q}^\star) &= [q_1(c_1), q_2(c_1), \cdots, q_n(c_1), q_1(c_2), q_2(c_2), \cdots, q_n(c_2), \cdots, q_1(c_s), q_2(c_s), \cdots, q_n(c_s)]^T, \\ \mathrm{vec}(F) &= [f_1(c_1), f_2(c_1), \cdots, f_n(c_1), f_1(c_2), f_2(c_2), \cdots, f_n(c_2), \cdots, f_1(c_s), f_2(c_s), \cdots, f_n(c_s)]^T, \\ \mathrm{vec}(G) &= [-p_1, -p_2, \cdots, -p_n, \underbrace{0, \cdots, 0}_{n(s-1)}]^T. \end{aligned}$$

For arbitrary matrices $A = (a_{ij})_{m\times n}$ and B, the Kronecker product $\otimes$ in equation (10) is defined as

$$A \otimes B = \begin{pmatrix} a_{11}B & a_{12}B & \cdots & a_{1n}B \\ a_{21}B & a_{22}B & \cdots & a_{2n}B \\ \vdots & \vdots & \ddots & \vdots \\ a_{m1}B & a_{m2}B & \cdots & a_{mn}B \end{pmatrix}. \tag{11}$$

3. Spectral collocation methods

For mechanical systems, the Euler–Lagrange equations are generally second-order nonlinear ODEs. In this section, we study the spectral collocation method for the following second-order initial value problem,

$$\begin{cases} \ddot{\mathbf{q}}(t) = \mathbf{f}(t, \mathbf{q}(t), \dot{\mathbf{q}}(t)), \ 0 < t \le T, \\ \mathbf{q}(t_0) = \mathbf{q}_0, \ \dot{\mathbf{q}}(t_0) = \dot{\mathbf{q}}_0, \end{cases} \qquad \mathbf{q} \in \mathbb{R}^n, \tag{12}$$

where

$$\begin{aligned} \mathbf{q}(t) &= [q_1(t), q_2(t), \cdots, q_n(t)], \\ \mathbf{f}(t, \mathbf{q}(t), \dot{\mathbf{q}}(t)) &= [f_1(t, \mathbf{q}(t), \dot{\mathbf{q}}(t)), f_2(t, \mathbf{q}(t), \dot{\mathbf{q}}(t)), \cdots, f_n(t, \mathbf{q}(t), \dot{\mathbf{q}}(t))]. \end{aligned}$$

3.1. Differentiation matrix for an arbitrary interval

Suppose $\tilde{q} \in C([-1,1],\mathbb{R})$, then on the interval $[-1,1]$, the Lagrange interpolation function which is based on the Chebyshev–Gauss–Lobatto points $\{x_\nu\}_{\nu=0}^{s}$ can be constructed as follows

$$\tilde{q}(x) = \sum_{\nu=0}^{s} \tilde{q}^{\nu} l_{\nu,s}(x), \qquad \tilde{q}^{\nu} = \tilde{q}(x_\nu), \tag{13}$$

where $l_{\nu,s}$ are the Lagrange basis polynomials defined by (7). Taking the r-th order derivative of (13), the value of $\tilde{q}^{(r)}$ at the Chebyshev–Gauss–Lobatto points can be expressed as follows

$$\tilde{q}^{(r)}(x_\nu) = \sum_{\nu=0}^{s} \tilde{q}^{\nu} l_{\nu,s}^{(r)}(x_\nu), \qquad r \in \mathbb{Z}^{+}. \tag{14}$$

Equation (14) can be written in matrix form as $\tilde{\mathcal{Q}}^{(r)} = \tilde{D}^{(r)} \cdot \tilde{\mathcal{Q}}$, i.e.,

$$\underbrace{\begin{pmatrix} \tilde{q}^{(r)}(x_0) \\ \tilde{q}^{(r)}(x_1) \\ \vdots \\ \tilde{q}^{(r)}(x_s) \end{pmatrix}}_{\tilde{\mathcal{Q}}^{(r)}_{[-1,1]}} = \underbrace{\begin{pmatrix} l_{0,s}^{(r)}(x_0) & l_{1,s}^{(r)}(x_0) & \cdots & l_{s,s}^{(r)}(x_0) \\ l_{0,s}^{(r)}(x_1) & l_{1,s}^{(r)}(x_1) & \cdots & l_{s,s}^{(r)}(x_1) \\ \vdots & \vdots & \ddots & \vdots \\ l_{0,s}^{(r)}(x_s) & l_{1,s}^{(r)}(x_s) & \cdots & l_{s,s}^{(r)}(x_s)) \end{pmatrix}}_{\tilde{D}^{(r)}} \underbrace{\begin{pmatrix} \tilde{q}(x_0) \\ \tilde{q}(x_1) \\ \vdots \\ \tilde{q}(x_s) \end{pmatrix}}_{\tilde{\mathcal{Q}}_{[-1,1]}}. \tag{15}$$

Now, consider q to be defined on the interval $[kh,(k+1)h]$. Let $\{c_\nu\}_{\nu=0}^{s} \in [kh,(k+1)h]$ be the rescaling and translation of the Chebyshev–Gauss–Lobatto points $\{x_\nu\}_{\nu=0}^{s} \in [-1,1]$. Then, the relationship between c_ν and x_ν is given by

$$c_\nu = kh + \frac{h}{2}(x_\nu + 1), \quad x_\nu = \frac{2}{h}(c_\nu - kh) - 1, \qquad \nu = 0,\ldots,s.$$

Let $\mathcal{Q} = [q(c_0),\cdots,q(c_s)]^T = \left[q\left(kh+\frac{h}{2}(x_0+1)\right),\cdots,q\left(kh+\frac{h}{2}(x_s+1)\right)\right]^T$. It is easy to show that $\mathcal{Q}^{(r)} = D^{(r)} \cdot \mathcal{Q}$ and here $D^{(r)}$ and $\tilde{D}^{(r)}$ are related by the following equality,

$$D_{i,j}^{(r)} = \left(\frac{2}{h}\right)^{r} \tilde{D}_{i,j}^{(r)}. \tag{16}$$

For the case $r=1$, the first-order Chebyshev differentiation matrix $\tilde{D}^{(1)}$ is given by [16],

$$\tilde{D}_{i,j}^{(1)} = \begin{cases} \frac{2s^2+1}{6}, & i=j=0, \\ \frac{-x_j}{2(1-x_j^2)}, & i=j=1,...,s-1, \\ \frac{\alpha_i(-1)^{(i+j)}}{\alpha_j(x_i-x_j)}, & i\neq j, \quad i,j=0,...,s, \\ -\frac{2s^2+1}{6}, & i=j=s, \end{cases} \qquad \alpha_l = \begin{cases} 2, & l=0 \text{ or } s, \\ 1, & \text{otherwise.} \end{cases} \tag{17}$$

Here, $\tilde{D}^{(1)}$ is a $(s+1)\times(s+1)$ matrix indexed from 0 to s. Higher-order Chebyshev differentiation matrices $\tilde{D}^{(r)}, (r \geqslant 2)$ can be obtained by raising the first-order differentiation matrix to the appropriate power, i.e.,

$$\tilde{D}^{(r)} = (\tilde{D}^{(1)})^{r}. \tag{18}$$

3.2. Multi-interval spectral collocation method

To solve (12), we first divide the interval $[0,T]$ into N subintervals of equal length h and apply the spectral collocation method in each subinterval $[kh,(k+1)h]$. By introducing the auxiliary variable $\mathbf{y} = \dot{\mathbf{q}}$, (12) can be written in the following form

$$\begin{cases} \dot{\mathbf{q}}(t) = \mathbf{y}, \\ \dot{\mathbf{y}}(t) = \mathbf{f}(t,\mathbf{q}(t),\mathbf{y}(t)), \end{cases} \tag{19}$$

with initial conditions $\mathbf{q}(t_0) = \mathbf{q}_k^0$, $\mathbf{y}(t_0) = \dot{\mathbf{q}}_k^0$. Then, (19) can be discretized by introducing the first-order Chebyshev differential matrix Λ in the interval $[kh,(k+1)h]$ as follows

$$\begin{cases} \Lambda \mathcal{Q}_k = Y_k^\star, \\ \Lambda Y_k = F(t, \mathcal{Q}_k^\star, Y_k^\star), \end{cases} \tag{20}$$

where

$$\begin{aligned} \mathcal{Q}_k &= [\mathbf{q}_k^0, \mathcal{Q}_k^\star]^T, \quad \mathcal{Q}_k^\star = [\mathbf{q}_k(t_1), \mathbf{q}_k(t_2), ..., \mathbf{q}_k(t_s)]^T, \\ Y_k &= [\mathbf{y}_k^0, Y_k^\star]^T, \quad Y_k^\star = [\mathbf{y}_k(t_1), \mathbf{y}_k(t_2), ..., \mathbf{y}_k(t_s)]^T, \\ F(t, Q_k^\star, Y_k^\star) &= [\mathbf{f}(t_1, \mathbf{q}_k(t_1), \mathbf{y}_k(t_1)), \mathbf{f}(t_2, \mathbf{q}_k(t_2), \mathbf{y}_k(t_2)), \ldots, \mathbf{f}(t_s, \mathbf{q}_k(t_s), \mathbf{y}_k(t_s))]^T. \end{aligned}$$

From (16), we know that

$$\Lambda = \frac{2}{h} \tilde{D}^{(1)}(1\!:\!s, 0\!:\!s). \tag{21}$$

Here, $\tilde{D}^{(1)}(1\!:\!s, 0\!:\!s)$ is the matrix obtained from the first-order Chebyshev differentiation matrix $\tilde{D}^{(1)}$ by eliminating the first row. As the initial values $\mathbf{q}_k^0$ and $\dot{\mathbf{q}}_k^0$ are given, (20) can be rewritten as follows:

$$\Lambda^\star \mathcal{Q}_k^\star + \lambda_0 \mathbf{q}_k^0 = Y_k^\star, \tag{22}$$

$$\Lambda^\star Y_k^\star + \lambda_0 \dot{\mathbf{q}}_k^0 = F(t, \mathcal{Q}_k^\star, Y_k^\star), \tag{23}$$

where $\Lambda = [\lambda_0, \Lambda^\star]$, λ_0 is the first column of Λ. Substituting (22) into (23) yields the following equation,

$$\Lambda^\star(\Lambda^\star \mathcal{Q}_k^\star + \lambda_0 \mathbf{q}_k^0) + \lambda_0 \dot{\mathbf{q}}_k^0 = F(t, \mathcal{Q}_k^\star, \Lambda^\star \mathcal{Q}_k^\star + \lambda_0 \mathbf{q}_k^0), \tag{24}$$

which is equivalent to the following set of equations,

$$(\Lambda^\star)^2 \otimes I_n \mathrm{vec}(\mathcal{Q}_k^\star) - \mathrm{vec}(F(t, \mathcal{Q}_k^\star, \Lambda^\star \mathcal{Q}_k^\star + \lambda_0 \mathbf{q}_k^0)) + \lambda_0 \otimes (\dot{\mathbf{q}}_k^0)^T + (\Lambda^\star \lambda_0) \otimes (\mathbf{q}_k^0)^T = 0. \tag{25}$$

Thus, $\mathrm{vec}(\mathcal{Q}_k^\star)$ can be obtained from (25) by using the Newton–Raphson iteration.

4. Linear stability of SVI and SC

In this part, we perform a brief linear stability analysis of the proposed spectral collocation methods and the corresponding spectral variational integrators. The stability properties of spectral variational integrators for some specific choices of polynomial approximations and numerical quadrature rules are discussed in [14]. In our discussion, we establish the stability matrix of SVI with an arbitrary number of interpolation and quadrature points.

Consider the simple harmonic oscillator with Lagrangian $L(q, \dot{q}) = \frac{1}{2}\dot{q}^2 - \frac{1}{2}\sigma^2 q^2$. Then, the Euler–Lagrange equations of the system are given by

$$\ddot{q} = -\sigma^2 q, \qquad \sigma > 0, \quad \sigma, q \in \mathbb{R}, \tag{26}$$

and the corresponding Hamilton's equations are given by

$$\begin{cases} \dot{q} &= p, \\ \dot{p} &= -\sigma^2 q. \end{cases}$$

4.1. Stability matrix of spectral variational integrator

The spectral variational integrator scheme, (8a) and (8b), applied to (26) can be written in the following matrix form:

$$\hat{A}_k \hat{\mathcal{Q}}_k + \hat{F}_k = \hat{G}_k, \tag{27}$$

where $\hat{A}_k$ is a $s \times (s+1)$ matrix whose entries are given by

$$\hat{A}_k^{i,j} = \frac{2}{h} \sum_{\mu=1}^{m} w_\mu \dot{l}_{i-1,s}(\tau_\mu) \dot{l}_{j-1,s}(\tau_\mu), \qquad i = 1, \ldots, s; \quad j = 1, \ldots, s+1,$$

$\hat{\mathcal{Q}}_k$ is a $(s+1)$-dimensional column vector

$$\hat{\mathcal{Q}}_k = [q_k^0, q_k^1, \cdots, q_k^s]^T,$$

$\hat{F}_k$ is a s-dimensional column vector

$$\begin{aligned}\hat{F}_k &= [f_k^0, f_k^1, \cdots, f_k^{s-1}]^T \\ &= \Big[\frac{h}{2}\sum_{\mu=1}^{m} w_\mu l_{0,s}(\tau_\mu)\cdot\frac{\partial L}{\partial q}, \frac{h}{2}\sum_{\mu=1}^{m} w_\mu l_{1,s}(\tau_\mu)\cdot\frac{\partial L}{\partial q}, \cdots, \frac{h}{2}\sum_{\mu=1}^{m} w_\mu l_{s-1,s}(\tau_\mu)\cdot\frac{\partial L}{\partial q}\Big]^T \\ &= \Big(-\frac{\sigma^2 h}{2}\Big)\Big[\sum_{\mu=1}^{m} w_\mu l_{0,s}(\tau_\mu)\sum_{\nu=0}^{s} q_k^\nu l_{\nu,s}(\tau_\mu), \cdots, \sum_{\mu=1}^{m} w_\mu l_{s-1,s}(\tau_\mu)\sum_{\nu=0}^{s} q_k^\nu l_{\nu,s}(\tau_\mu)\Big]^T,\end{aligned}$$

and $\hat{G}_k$ is a s-dimensional column vector

$$\hat{G}_k = [-p_k, \mathbf{0}_{1\times(s-1)}]^T.$$

Partition $\hat{A}_k$, $\hat{\mathcal{Q}}_k$ and $\hat{F}_k$ as follows:

$$\begin{aligned}&\hat{A}_k = \frac{2}{h}\hat{\mathcal{A}}_k = \frac{2}{h}[\mathcal{A}_k^0, \mathcal{A}_k^\star], \\ &\hat{\mathcal{Q}}_k = [q_k, \mathcal{Q}_k^\star], \\ &\hat{F}_k = \Big(-\frac{\sigma^2 h}{2}\Big)\hat{\mathcal{F}}_k\hat{\mathcal{Q}}_k = \Big(-\frac{\sigma^2 h}{2}\Big)[\mathcal{F}_k^0, \mathcal{F}_k^\star]\hat{\mathcal{Q}}_k,\end{aligned}$$

where $\mathcal{A}_k^0$ is the first column of $\hat{\mathcal{A}}_k$, $\mathcal{A}_k^\star$ is the remaining part of $\hat{\mathcal{A}}_k$, $\mathcal{F}_k^0$ is the first column of $\hat{\mathcal{F}}_k$, $\mathcal{F}_k^\star$ is the remaining part of $\hat{\mathcal{F}}_k$, and $\hat{\mathcal{F}}_k$ is a $s\times(s+1)$ matrix whose entries are given by

$$\hat{\mathcal{F}}_k^{i,j} = \sum_{\mu=1}^{m} w_\mu l_{i-1,s}(\tau_\mu) l_{j-1,s}(\tau_\mu), \qquad i = 1,\ldots,s; \quad j = 1,\ldots,s+1.$$

Then, (27) can be rewritten in the following form:

$$\frac{2}{h}[\mathcal{A}_k^0, \mathcal{A}_k^\star]\cdot[q_k, \mathcal{Q}_k^\star] - \frac{\sigma^2 h}{2}[\mathcal{F}_k^0, \mathcal{F}_k^\star]\cdot[q_k, \mathcal{Q}_k^\star] - \hat{G}_k = 0,$$

or equivalently,

$$\frac{2}{h}\mathcal{A}_k^\star\mathcal{Q}_k^\star + \frac{2}{h}\mathcal{A}_k^0 q_k - \frac{\sigma^2 h}{2}\mathcal{F}_k^\star\mathcal{Q}_k^\star - \frac{\sigma^2 h}{2}\mathcal{F}_k^0 q_k - \hat{G}_k = 0.$$

So, $\mathcal{Q}_k^\star$ is given by

$$\mathcal{Q}_k^\star = \Big(4\mathcal{A}_k^\star - \sigma^2 h^2\mathcal{F}_k^\star\Big)^{-1}\Big[\Big(-4\mathcal{A}_k^0 + \sigma^2 h^2\mathcal{F}_k^0\Big)q_k + 2h\hat{G}_k\Big]. \tag{28}$$

Then, q_{k+1} can be obtained as follows

$$q_{k+1} = q_k^s = \Big(4\mathcal{A}_k^\star - z\mathcal{F}_k^\star\Big)^{-1}(s,:)\Big(-4\mathcal{A}_k^0 + z\mathcal{F}_k^0\Big)\cdot q_k - 2\Big(4\mathcal{A}_k^\star - z\mathcal{F}_k^\star\Big)^{-1}(s,1)\cdot hp_k, \qquad z = \sigma^2 h^2, \tag{29}$$

and p_{k+1} can be derived from (8c),

$$p_{k+1} = \sum_{\mu=1}^{m} w_\mu\Big[\frac{h}{2}l_{s,s}(\tau_\mu)\cdot(-\sigma^2)\sum_{\nu=0}^{s} q_k^\nu l_{\nu,s}(\tau_\mu) + \dot{l}_{s,s}(\tau_\mu)\cdot\frac{2}{h}\sum_{\nu=0}^{s} q_k^\nu \dot{l}_{\nu,s}(\tau_\mu)\Big], \tag{30}$$

which is equivalent to

$$hp_{k+1} = \Big(-\frac{z}{2}\Big)\sum_{\mu=1}^{m} w_\mu l_{s,s}(\tau_\mu)\sum_{\nu=0}^{s} q_k^\nu l_{\nu,s}(\tau_\mu) + 2\sum_{\mu=1}^{m} w_\mu \dot{l}_{s,s}(\tau_\mu)\sum_{\nu=0}^{s} q_k^\nu \dot{l}_{\nu,s}(\tau_\mu) \triangleq \mathcal{B}_k\mathcal{Q}_k, \tag{31}$$

where $\mathcal{B}_k$ is a $(s+1)$-dimensional column vector whose entries are given by

$$\mathcal{B}_k^{(j)} = -\frac{z}{2}\sum_{\mu=1}^{m} w_\mu l_{s,s}(\tau_\mu) l_{j-1,s}(\tau_\mu) + 2\sum_{\mu=1}^{m} w_\mu \dot{l}_{s,s}(\tau_\mu)\dot{l}_{j-1,s}(\tau_\mu).$$

Here, $\mathcal{B}_k^{(j)}$ denotes the j-th column of $\mathcal{B}_k$. Inserting (28) into (31), we get

$$hp_{k+1} = \mathcal{B}_k^0 q_k + \mathcal{B}_k^\star \mathcal{Q}_k^\star \quad = [\mathcal{B}_k^0 + \mathcal{B}_k^\star (4\mathcal{A}_k^\star - z\mathcal{F}_k^\star)^{-1}(-4\mathcal{A}_k^0 + z\mathcal{F}_k^0)] \cdot q_k - 2\mathcal{B}_k^\star (4\mathcal{A}_k^\star - z\mathcal{F}_k^\star)^{-1}(\mathtt{s},1) \cdot hp_k \tag{32}$$

where $\mathcal{B}_k^0$ is the first column of $\mathcal{B}_k$, $\mathcal{B}_k^\star$ is the remaining part of $\mathcal{B}_k$. Equalities (29) and (32) can be expressed in the following matrix form:

$$\begin{pmatrix} q_{k+1} \\ h\dot{q}_{k+1} \end{pmatrix} = S_1(z) \begin{pmatrix} q_k \\ h\dot{q}_k \end{pmatrix}, \qquad z = \sigma^2 h^2, \tag{33}$$

where the stability matrix $S_1(z)$ is given by

$$S_1(z) = \begin{pmatrix} (4\mathcal{A}_k^\star - z\mathcal{F}_k^\star)^{-1}(\mathtt{s},:)(-4\mathcal{A}_k^0 + z\mathcal{F}_k^0) & -2(4\mathcal{A}_k^\star - z\mathcal{F}_k^\star)^{-1}(\mathtt{s},1) \\ \mathcal{B}_k^0 + \mathcal{B}_k^\star (4\mathcal{A}_k^\star - z\mathcal{F}_k^\star)^{-1}(-4\mathcal{A}_k^0 + z\mathcal{F}_k^0) & -2\mathcal{B}_k^\star (4\mathcal{A}_k^\star - z\mathcal{F}_k^\star)^{-1}(\mathtt{s},1) \end{pmatrix}. \tag{34}$$

4.2. Stability matrix of spectral collocation method

The spectral collocation scheme applied to (26) can be easily derived from (24) and it has the form

$$\Lambda^\star(\Lambda^\star \mathcal{Q}_k^\star + \lambda_0 q_k) + \lambda_0 \dot{q}_k = -\sigma^2 \mathcal{Q}_k^\star, \tag{35}$$

where

$$\begin{cases} q_{k+1} = \mathcal{Q}_k^\star(\mathtt{s},:), \\ \dot{q}_{k+1} = \Lambda^\star(\mathtt{s},:)\,\mathcal{Q}_k^\star + \lambda_0(\mathtt{s})\,q_k. \end{cases}$$

From (21), we know that

$$\Lambda^\star = \frac{2}{h}\tilde{D}^{(1)}(1:\mathtt{s},1:\mathtt{s}) \triangleq \frac{2}{h}\mathcal{D}_\star, \qquad \lambda_0 = \frac{2}{h}\tilde{D}^{(1)}(1:\mathtt{s},0) \triangleq \frac{2}{h}\mathcal{D}_0.$$

Then, (35) can be rewritten as

$$\frac{2}{h}\mathcal{D}_\star\Big(\frac{2}{h}\mathcal{D}_\star \mathcal{Q}_k^\star + \frac{2}{h}\mathcal{D}_0 q_k\Big) + \frac{2}{h}\mathcal{D}_0 \dot{q}_k = -\sigma^2 \mathcal{Q}_k^\star,$$

and q_{k+1}, $\dot{q}_{k+1}$ can be obtained as follows

$$\begin{cases} q_{k+1} = -(4\mathcal{D}_\star^2 + \sigma^2 h^2 I_s)^{-1}(\mathtt{s},:) \cdot (2h\mathcal{D}_0 \dot{q}_k + 4\mathcal{D}_\star \mathcal{D}_0 q_k), \\ h\dot{q}_{k+1} = -2\mathcal{D}_\star(\mathtt{s},:) \cdot (4\mathcal{D}_\star^2 + \sigma^2 h^2 I_s)^{-1}(2h\mathcal{D}_0 \dot{q}_k + 4\mathcal{D}_\star \mathcal{D}_0 q_k) + 2\mathcal{D}_0(\mathtt{s})\,q_k. \end{cases}$$

Thus, we have

$$\begin{pmatrix} q_{k+1} \\ h\dot{q}_{k+1} \end{pmatrix} = S_2(z) \begin{pmatrix} q_k \\ h\dot{q}_k \end{pmatrix}, \qquad z = \sigma^2 h^2, \tag{36}$$

where the stability matrix $S_2(z)$ is given by

$$S_2(z) = \begin{pmatrix} -4(4\mathcal{D}_\star^2 + zI_s)^{-1}(\mathtt{s},:)\,\mathcal{D}_\star \mathcal{D}_0 & -2(4\mathcal{D}_\star^2 + zI_s)^{-1}(\mathtt{s},:)\,\mathcal{D}_0 \\ -8\tilde{\mathcal{D}}(\mathtt{s},:)(4\mathcal{D}_\star^2 + zI_s)^{-1}\mathcal{D}_\star \mathcal{D}_0 + 2\mathcal{D}_0(\mathtt{s}) & -4\mathcal{D}_\star(\mathtt{s},:)(4\mathcal{D}_\star^2 + zI_s)^{-1}\mathcal{D}_0 \end{pmatrix}. \tag{37}$$

Now, we recall the various notions of stability in terms of the stability matrix S:

Definition 4.1. ([10,18,2,13]) For equation (26) and its stability matrix $S(z)$, $z = \sigma^2 h^2$,

(1) $R_s = \{z \in \mathbb{R} | z > 0 \text{ and } \rho(S) \le 1\}$ is called the stability region,
(2) $R_p = \{z \in \mathbb{R} | z > 0,\ \rho(S) = 1 \text{ and } \mathrm{tr}(S)^2 < 4\det(S)\}$ is called the periodicity region,
(3) $R_q = \{z \in \mathbb{R} | z > 0, \text{ and } \det(S) < 1,\ |\mathrm{tr}(S)| < \det(S) + 1\}$ is called the strong stability region,
(4) If $\{z \in (0, +\infty)\} \subset R_s$, the method is called A-stable,
(5) If $\{z \in (0, +\infty)\} \subset R_p$, the method is called P-stable.

The linear stabilities of SVI and SC are mainly determined by their stability matrices $S_1(z)$ and $S_2(z)$, given by (34) and (37), respectively. These formulas allow the users of SVI and SC to compute the stability regions of the proposed numerical methods. For different kinds of interpolants and numerical quadrature rules, the specific form of $S_1(z)$ and $S_2(z)$ might be different, but the procedure for deriving them will be similar.

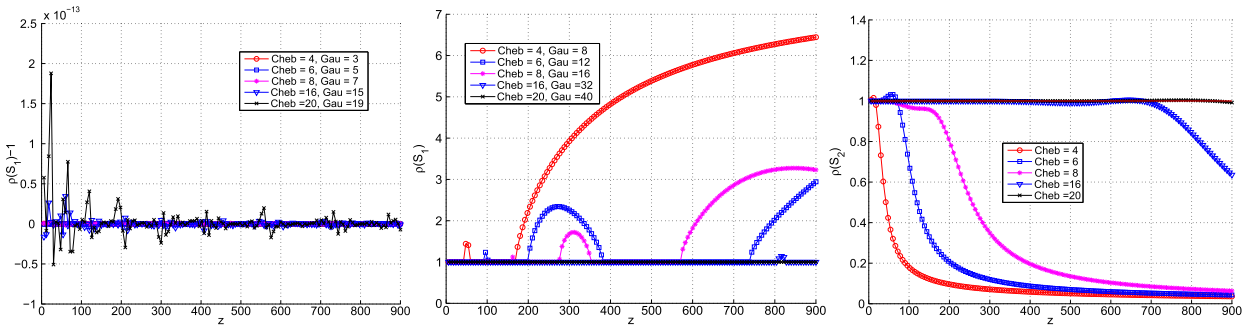

Fig. 3. Simple harmonic oscillator. Spectral radius $\rho(S(z))$ of SVI (left and middle) and SC (right) for $z \in [0, 900]$. Here, 'Cheb' means the number of Chebyshev–Gauss–Lobatto interpolation points and 'Gau' means the number of Gauss–Legendre quadrature points.

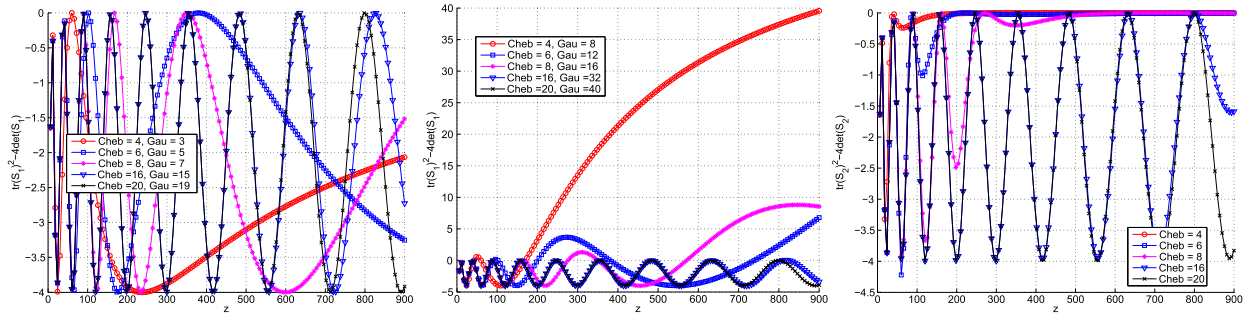

Fig. 4. Simple harmonic oscillator. $\mathrm{tr}(S)^2 - 4\det(S)$ of SVI (left and middle) and SC (right) for $z \in [0, 900]$. Here, 'Cheb' means the number of Chebyshev–Gauss–Lobatto interpolation points and 'Gau' means the number of Gauss–Legendre quadrature points.

5. Numerical experiments

In this section, we demonstrate the stability, convergence and accuracy of the proposed vectorized numerical realizations of SVI and SC applied to some classical mechanical systems, where the nonlinear equations are solved using the Newton method. The numerical simulations were carried out on a personal computer with an Intel Core i5-4210U, 1.70 GHz CPU, 8G RAM and the algorithms were implemented using Matlab 2014a.

5.1. Simple harmonic oscillator

Choosing initial values $q_0 = 0,\ p_0 = 1$, we simulate the simple harmonic problem (26) with both the spectral variational integrator and spectral collocation method. Figs. 3, 4, 5 and 6 show the value of $\rho(S)$, $\mathrm{tr}(S) - 4\det(S)$, $\det(S)$ and $|\mathrm{tr}(S)| - \det(S) - 1$ of SVI and SC for different $z \in [0, 900]$. Denote the number of chosen Chebyshev–Gauss–Lobatto points by s and let the number of Gauss quadrature points be $s - 1$ (left column of Figs. 3, 4, 5 and 6) and $2s$ (middle column of Figs. 3, 4, 5 and 6). It can be easily observed by comparing the first two columns of Figs. 3, 4, 5 and 6 that the stability properties of SVI are determined by both the number of interpolation points and the number of quadrature points. Let $\mathbf{x}_k = [\mathbf{q}, \dot{\mathbf{q}}]^T$ denote the state of a Hamiltonian system. To compute this system correctly [1], we should ensure that the determinant of the matrix $\frac{\partial \mathbf{x}_{k+1}}{\partial \mathbf{x}_k}$ is equal to 1, i.e., $\det(\frac{\partial \mathbf{x}_{k+1}}{\partial \mathbf{x}_k}) = 1$. As shown in Fig. 5, the determinants of S_1 are always equal to 1 to machine accuracy which guarantees the symplecticity of SVI, while the determinants of S_2 decrease rapidly as z increases. The performance of SVI when solving some high-dimensional stiff ordinary differential equations was studied in [8].

Fig. 7 gives a comparison of phase space trajectories computed using SVI and SC. The phase space trajectory for the simple harmonic oscillator computed using SVI is more symmetric than the trajectory obtained using SC. Fig. 8 shows the position error of these two methods. We can see that the position error of SC is larger and grows faster than SVI when they both use the same number of Chebyshev–Gauss–Lobatto points and the same step-size. From Fig. 9, we can see that the energy error of SC is also larger and grows faster than SVI. Figs. 10, 11, 12 compare the absolute error in position and energy between both methods under N-refinement and h-refinement, where N represents the number of Chebyshev–Gauss–Lobatto points and h represents the step-size. Fig. 10 shows the geometric convergence of both SVI and SC. The relative computation efficiencies of SVI, SC and some conventional symplectic methods have been discussed in [6,9].

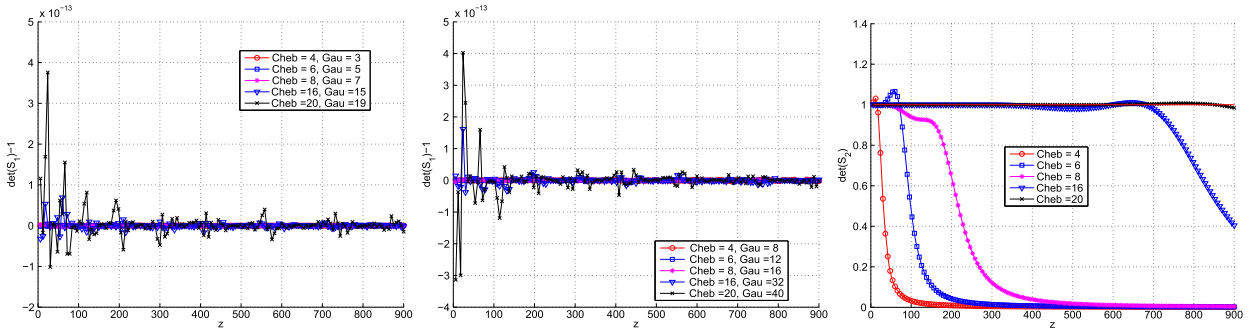

Fig. 5. Simple harmonic oscillator. $\det(S(z))$ of SVI (left and middle) and SC (right) for $z \in [0, 900]$. Here, 'Cheb' means the number of Chebyshev–Gauss–Lobatto interpolation points and 'Gau' means the number of Gauss–Legendre quadrature points.

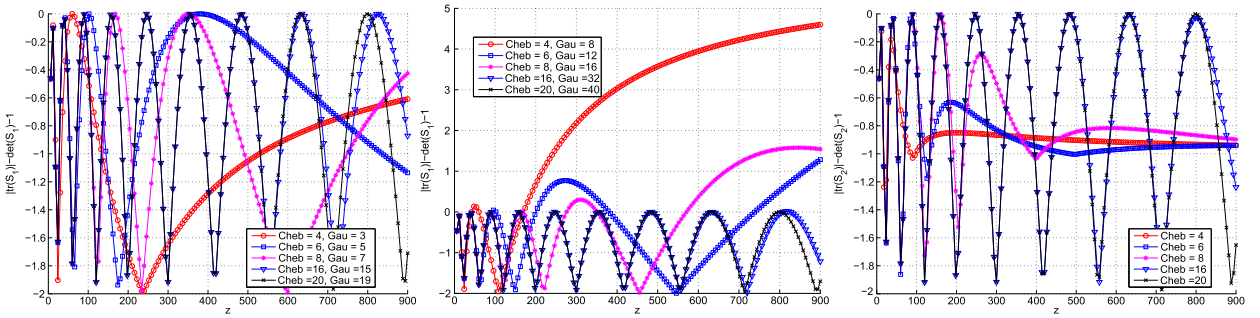

Fig. 6. Simple harmonic oscillator. $|\mathrm{tr}(S)| - \det(S) - 1$ of SVI (left and middle) and SC (right) for $z \in [0, 900]$. Here, 'Cheb' means the number of Chebyshev–Gauss–Lobatto interpolation points and 'Gau' means the number of Gauss–Legendre quadrature points.

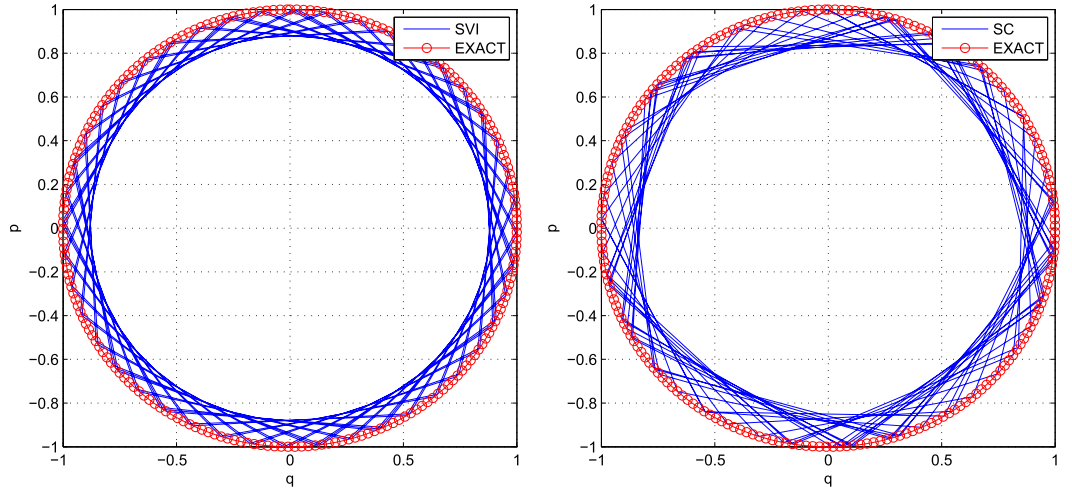

Fig. 7. Simple harmonic oscillator $\sigma = 1$. Left: The phase space trajectory computed by SVI with 9 point Chebyshev interpolation, 18 point Gauss–Legendre quadrature. Right: The phase space trajectory computed by SC also with 9 Chebyshev–Gauss–Lobatto points. For both methods, we choose step-size $h = 1$ and total time $T = 100$.

5.2. Kepler two-body problem

Now, we apply the spectral variational integrator and spectral collocation method to the Kepler two-body problem which describes the motion of two bodies under mutual gravitational attraction. If one body is placed at the origin, the corresponding angular momentum, Lagrangian and energy of the Kepler two-body system are given by

$$M(q, v) = q_1 v_2 - q_2 v_1,$$

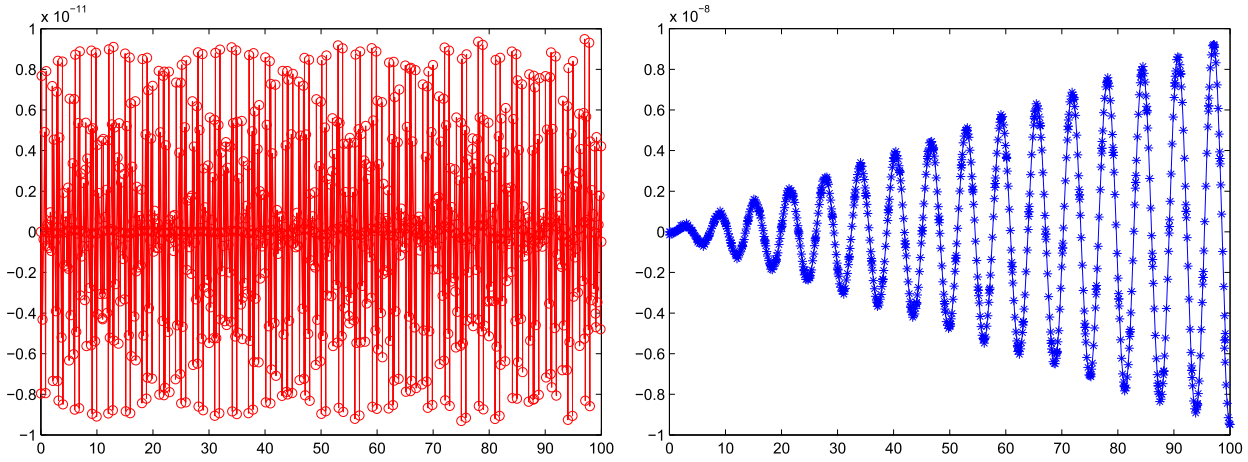

Fig. 8. Simple harmonic oscillator $\sigma = 1$. Left: Error in q computed by SVI with 9 point Chebyshev interpolation, 18 point Gauss–Legendre quadrature. Right: Error in q computed by SC also with 9 Chebyshev–Gauss–Lobatto points. For both methods, we choose step-size $h = 1$ and total time $T = 100$.

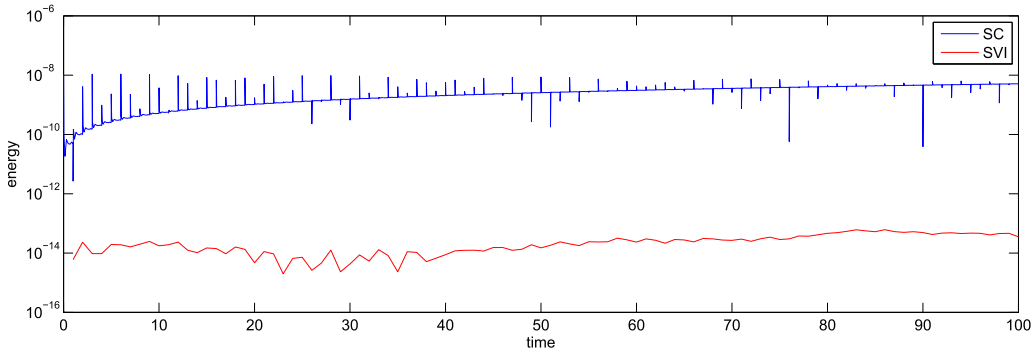

Fig. 9. Simple harmonic oscillator $\sigma = 1$. Absolute energy error for SVI with 9 point Chebyshev interpolation, 18 point Gauss–Legendre quadrature and SC with 9 Chebyshev–Gauss–Lobatto points. For both methods, we choose step-size $h = 1$ and total time $T = 100$.

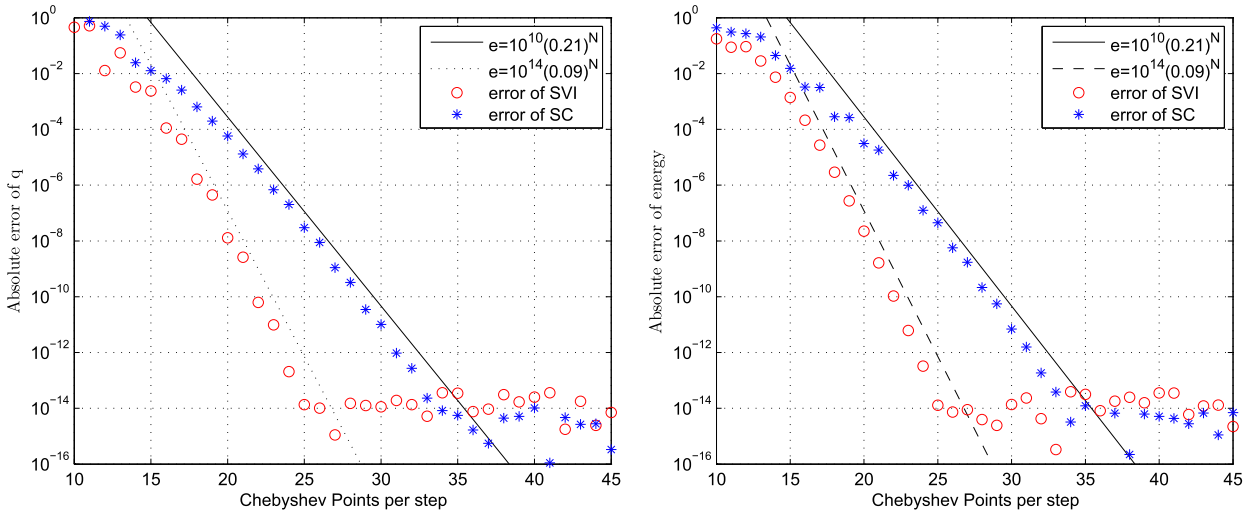

Fig. 10. Geometric convergence of the simple harmonic oscillator $\sigma = 1$. Left: Maximum absolute error of q for both SVI and SC with N-refinement. Right: Maximum absolute error of energy for both SVI and SC with N-refinement. For SVI, we choose the number of Gauss–Legendre quadrature points to be twice the number of Chebyshev–Gauss–Lobatto points.

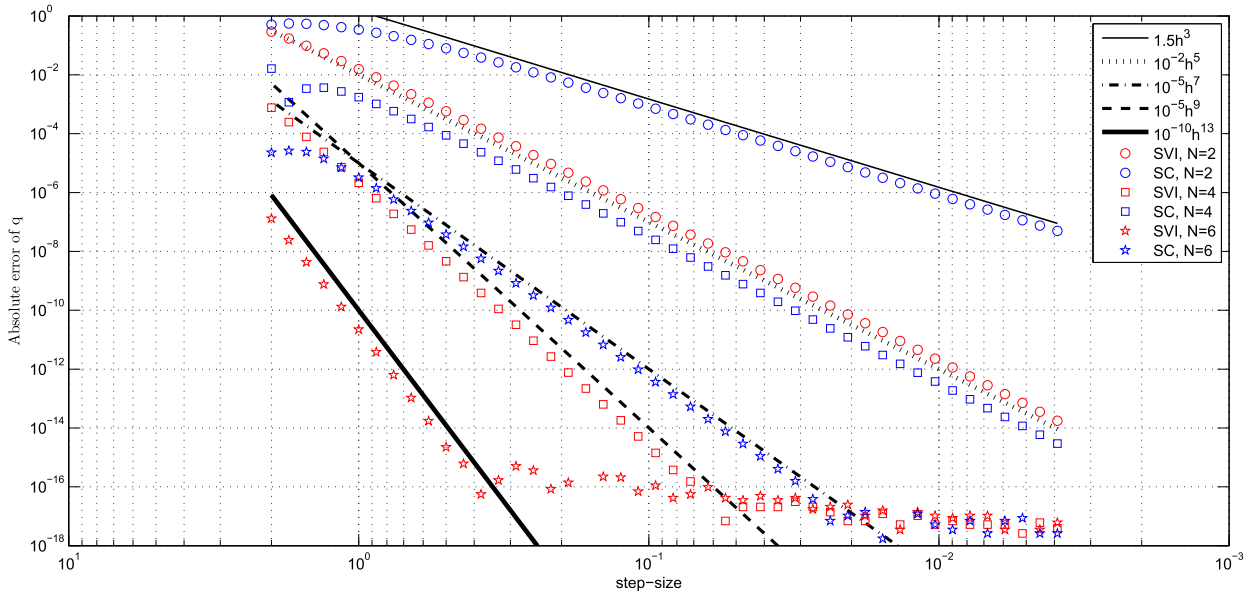

Fig. 11. Simple harmonic oscillator $\sigma = 1$. Maximum absolute error of q for both SVI and SC with h-refinement. For SVI, we choose the number of Gauss–Legendre quadrature points to be twice the number of Chebyshev–Gauss–Lobatto points.

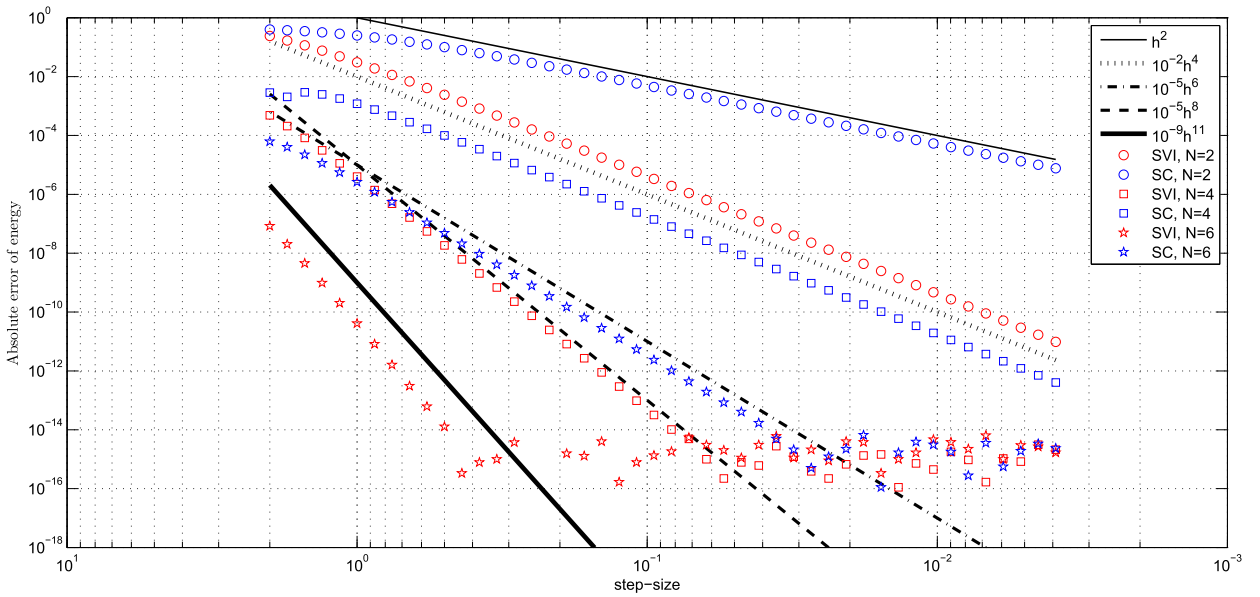

Fig. 12. Simple harmonic oscillator $\sigma = 1$. Maximum absolute error of energy for both SVI and SC with h-refinement. For SVI, we choose the number of Gauss–Legendre quadrature points to be twice the number of Chebyshev–Gauss–Lobatto points.

$$L(q, v) = T - V = \frac{1}{2}(v_1^2 + v_2^2) + \frac{1}{\sqrt{q_1^2 + q_2^2}},$$

and

$$E(q, v) = \frac{1}{2}(v_1^2 + v_2^2) - \frac{1}{\sqrt{q_1^2 + q_2^2}},$$

respectively. Here, $q = (q_1, q_2)$ represents the position of the second body and $v = (v_1, v_2)$ represents the velocity. Using (2), we can easily obtain the Euler–Lagrange equations of the system, expressed in first-order form,

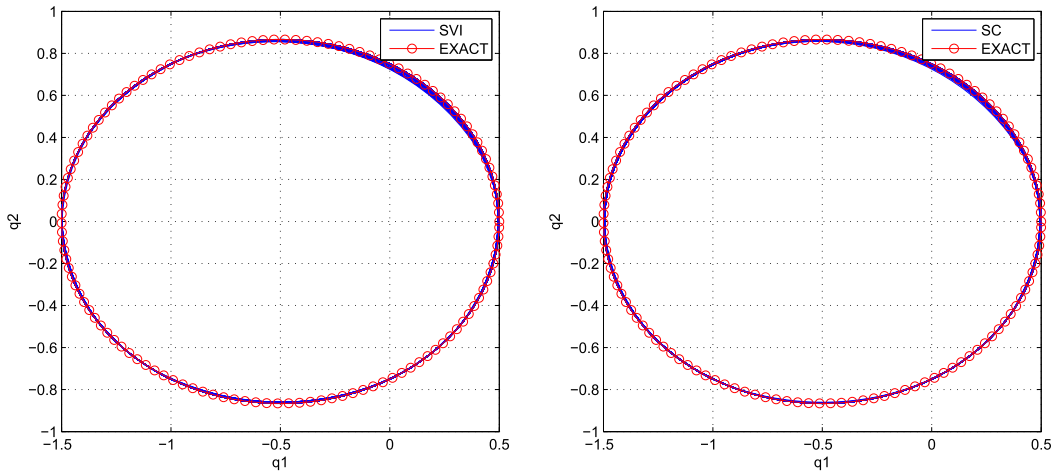

Fig. 13. Kepler two-body problem. Left: orbit computed by SVI with 6 point Chebyshev interpolation and 12 point Gauss–Legendre quadrature. Right: orbit computed by SC with 6 Chebyshev–Gauss–Lobatto points. For both methods, we choose eccentricity $e = 0.5$, step-size $h = 0.2$ and total time $T = 2000$.

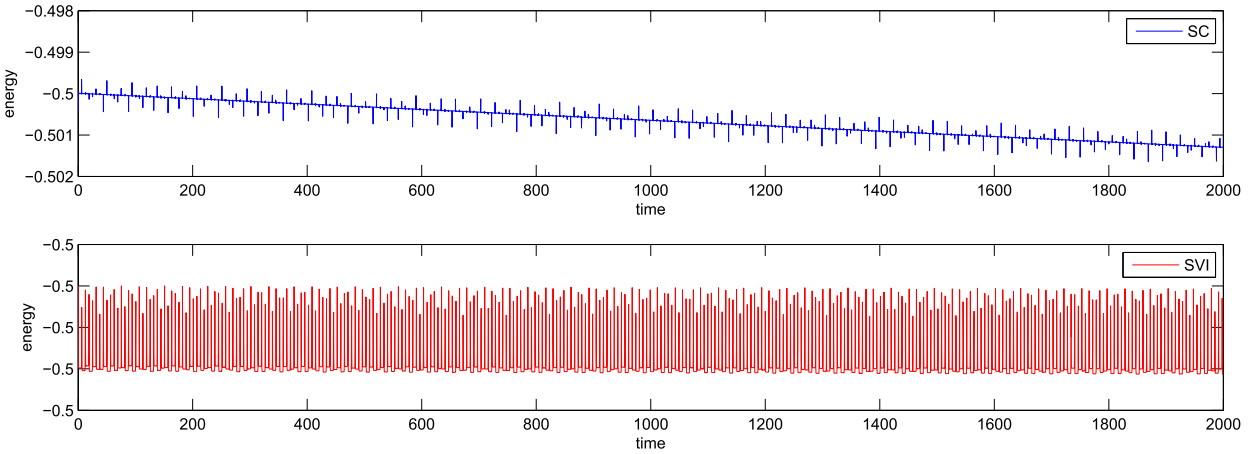

Fig. 14. Kepler two-body problem. Top: Energy computed by SC with 6 Chebyshev–Gauss–Lobatto points. Bottom: Energy computed by SVI with 6 point Chebyshev interpolation and 12 point Gauss–Legendre quadrature. For both methods, we choose eccentricity $e = 0.5$, step-size $h = 0.2$ and total time $T = 2000$.

$$\begin{aligned} \dot{q}_1 &= v_1, \\ \dot{q}_2 &= v_2, \\ \dot{v}_1 &= -\frac{q_1}{(q_1^2+q_2^2)^{3/2}}, \\ \dot{v}_2 &= -\frac{q_2}{(q_1^2+q_2^2)^{3/2}}. \end{aligned} \tag{38}$$

The analytic solution of (38) is 2π-periodic. Choosing initial conditions

$$q_1(0) = 1-e,\ \ q_2(0) = 0,\ \ v_1(0) = 0,\ \ v_2(0) = \sqrt{\frac{1+e}{1-e}}\ \ (0 \le e < 1),$$

the energy $E_0 = -0.5$ and the momentum $M_0 = \sqrt{1-e^2}$ are conserved.

Fig. 13 shows the orbits of the Kepler two-body system computed by SVI and SC, both with 6 Chebyshev–Gauss–Lobatto points. The orbit computed by SVI is more symmetric than the orbit computed by SC. Fig. 14 and 15 give the energy and angular momentum comparisons of both two methods separately. We can see that SVI preserves both energy and angular momentum very well, while the energy and angular momentum drift when computed by SC. Fig. 16 and 17 give the comparisons of the position error of Kepler two-body problem computed by SVI and SC under N-refinement and h-refinement. According to the numerical results, it is not hard to see that SVI is superior to SC in terms of the accuracy of position, energy and angular momentum when using the same number of Chebyshev–Gauss–Lobatto points and step-size.

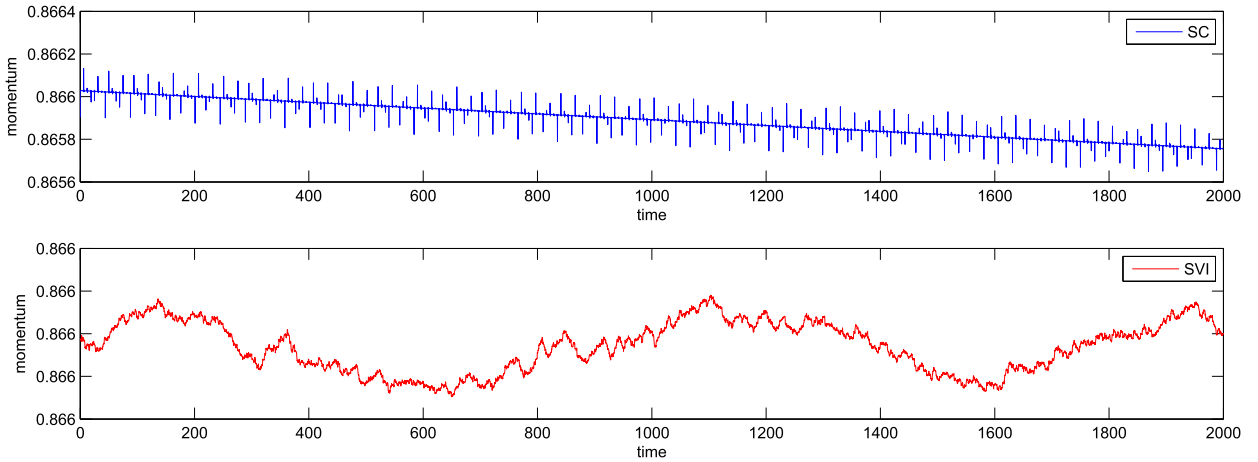

Fig. 15. Kepler two-body problem. Top: Angular momentum computed by SC with 6 Chebyshev–Gauss–Lobatto points. Bottom: Angular momentum computed by SVI with 6 point Chebyshev interpolation and 12 point Gauss–Legendre quadrature. For both methods, we choose eccentricity $e = 0.5$, step-size $h = 0.2$ and total time $T = 2000$.

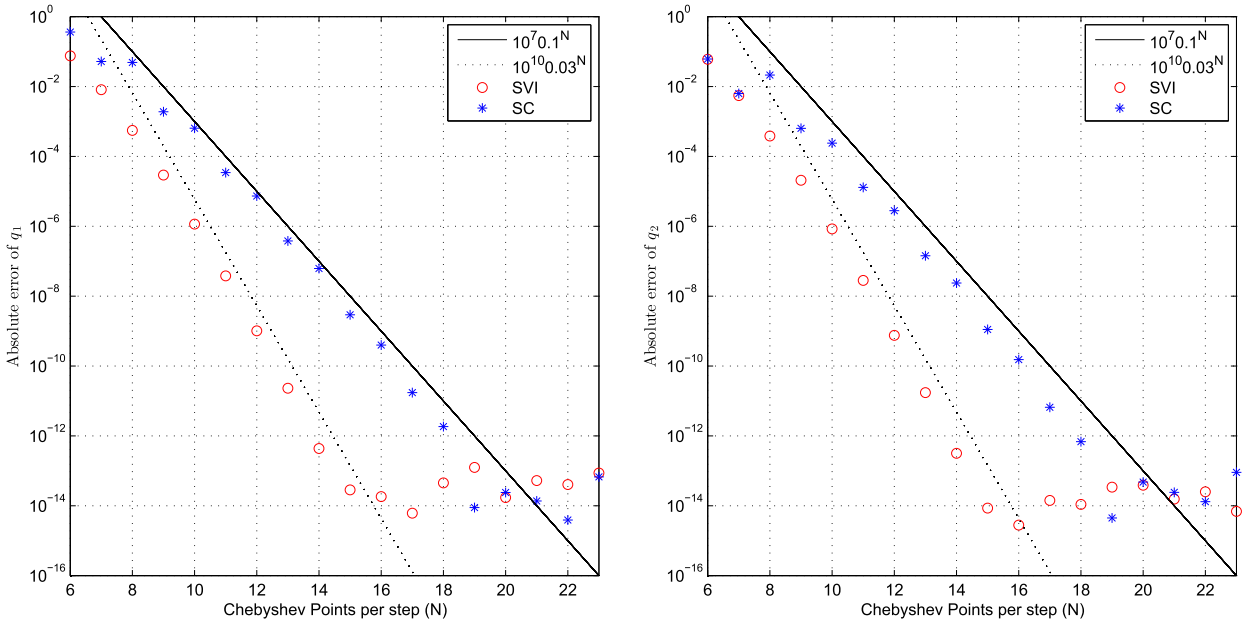

Fig. 16. Geometric convergence of the Kepler two-body problem. Comparison of the maximum absolute error of q_1 and q_2 computed by SVI and SC with N-refinement. For SVI, we choose the number of Gauss–Legendre quadrature points to be twice the number of Chebyshev–Gauss–Lobatto points.

The numerical experiments demonstrate that the accuracy of spectral variational integrators increases with the number of Chebyshev points. However, the accuracy of the discrete Lagrangian depends on both the polynomial order of the approximation space, as well as the accuracy of the quadrature rule. As such, we have to refine both the approximation space and the quadrature rule concurrently. Since the quadrature rule is used to approximate the action integral, the required number of quadrature points m depends on both the number of interpolation points s as well as the form of the Lagrangian function $L(q, \dot{q})$. In order to ensure that the accuracy of our spectral variational integrators are not limited by the accuracy of the quadrature rule, we have chosen to use a relatively large number of Gauss–Legendre quadrature points, i.e., $m = 2s$, but a smaller number of quadrature points may be sufficient for other Lagrangians.

6. Conclusion

In this paper, we construct vectorized numerical realizations of the spectral collocation method and the Galerkin spectral variational integrator. The linear stability of both methods is also discussed, and we obtain analytical expressions for the stability matrices for both methods. From the numerical comparisons of spectral variational integrators and spectral collocation methods, we can see that both methods converge geometrically and SVI is more accurate in position, angular

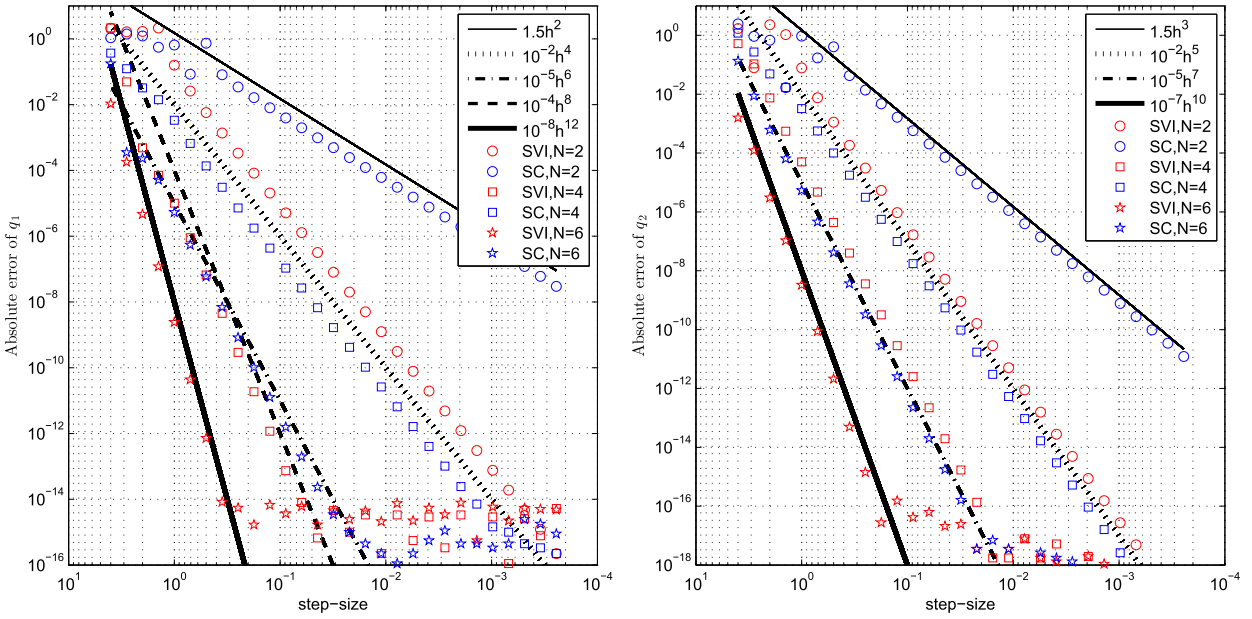

Fig. 17. Kepler two-body problem. Comparison of the maximum absolute error of q_1 and q_2 computed by SVI and SC with h-refinement. For SVI, we choose the number of Gauss–Legendre quadrature points to be twice the number of Chebyshev–Gauss–Lobatto points.

momentum and energy than SC, when using the same number of Chebyshev–Gauss–Lobatto points and the same step-size. Our future exploration will focus on extending the synthesis of variational integrators and spectral methods to construct efficient high-order numerical schemes for partial differential equations and on analyzing the stability properties of these methods.

Acknowledgements

YQL was supported in part by the National Postdoctoral Program for Innovative Talents, NSFC Grants No. 51327801, 51475195, 91748204, and National Key Research and Development Program of China Grant 2017YFB1301504. BYW was supported in part by the NSFC Grant No. 11271100. ML was supported in part by NSF Grants CMMI-1029445, DMS-1065972, CMMI-1334759, DMS-1345013, DMS-1411792, and NSF CAREER Award DMS-1010687.

References

[1] K. Feng, M. Qin, Symplectic Geometric Algorithms for Hamiltonian Systems, Springer, Berlin, Heidelberg, 2010.
[2] J.M. Franco, Stability of explicit ARKN methods for perturbed oscillators, J. Comput. Appl. Math. 173 (2) (2005) 389–396.
[3] B. Gladman, M. Duncan, J. Candy, Symplectic integrators for long-term integrations in celestial mechanics, Celest. Mech. Dyn. Astron. 52 (3) (1991) 221–240.
[4] E. Hairer, C. Lubich, G. Wanner, Structure-preserving algorithms for ordinary differential equations, in: Geometric Numerical Integration, second edition, in: Springer Series in Computational Mathematics, vol. 31, Springer-Verlag, Berlin, 2006.
[5] J. Hall, M. Leok, Spectral variational integrators, Numer. Math. 130 (4) (2015) 681–740.
[6] N. Kanyamee, Z. Zhang, Comparison of a spectral collocation method and symplectic methods for Hamiltonian systems, Int. J. Numer. Anal. Model. 8 (1) (2011) 86–104.
[7] B. Leimkuhler, S. Reich, Simulating Hamiltonian Dynamics, Cambridge University Press, 2004.
[8] Y.Q. Li, B.Y. Wu, M. Leok, Spectral variational integrators for semi-discrete hamiltonian wave equations, J. Comput. Appl. Math. 325 (2017) 56–73.
[9] Y.Q. Li, B.Y. Wu, Melvin Leok, Spectral-collocation variational integrators, J. Comput. Phys. 332 (2017) 83–98.
[10] W.J. Liu, B.Y. Wu, J.B. Sun, Some numerical algorithms for solving the highly oscillatory second-order initial value problems, J. Comput. Phys. 276 (2014) 235–251.
[11] J.E. Marsden, T.S. Ratiu, Introduction to Mechanics and Symmetry: a Basic Exposition of Classical Mechanical Systems, Texts in Applied Mathematics, Springer, 1999.
[12] J.E. Marsden, M. West, Discrete mechanics and variational integrators, Acta Numer. 10 (2001) 357–514.
[13] R.I. McLachlan, Y. Sun, P.S.P. Tse, Linear stability of partitioned Runge–Kutta methods, SIAM J. Numer. Anal. 49 (1) (February 2011) 232–263.
[14] S. Ober-Blöbaum, N. Saake, Construction and analysis of higher order Galerkin variational integrators, Adv. Comput. Math. (2014).
[15] Y.L. Sachkov, A.A. Agrachev, Control Theory from the Geometric Viewpoint, 1st edition, Springer, Berlin, Heidelberg, 2004.
[16] L.N. Trefethen, Spectral Methods in MATLAB, Software, Environments and Tools, vol. 10, Society for Industrial and Applied Mathematics (SIAM), Philadelphia, PA, 2000.
[17] L.N. Trefethen, Approximation Theory and Approximation Practice, Society for Industrial and Applied Mathematics (SIAM), Philadelphia, PA, 2013.
[18] X.Y. Wu, X. You, B. Wang, Structure-Preserving Algorithms for Oscillatory Differential Equations, Springer Publishing Company, Incorporated, 2013.